Proteasome dysfunction under compromised redox metabolism dictates liver injury in NASH through ASK1/PPARγ binodal complementary modules

Debajyoti Das [a], Avishek Paul [a], Abhishake Lahiri [b], Moumita Adak [a], Sujay K. Maity [a], Ankita Sarkar [a], Sandip Paul [b,c], Partha Chakrabarti [a,1,*]

[a] *Division of Cell Biology and Physiology, CSIR-Indian Institute of Chemical Biology, Kolkata, India*
[b] *Division of Structural Biology & Bioinformatics, CSIR-Indian Institute of Chemical Biology, Kolkata, India*
[c] *JIS Institute of Advanced Studies and Research, JIS University, Kolkata, India*

ABSTRACT

Incidence of hepatotoxicity following acute drug-induced proteasomal inhibition and development of chronic proteasome dysfunction in obesity and insulin resistance underscores the crucial importance of hepatic protein homeostasis albeit with an elusive molecular basis and therapeutic opportunities. Apart from lipotoxicity and endoplasmic reticulum (ER) stress, herein we report that hepatocytes are highly susceptible to proteasome-associated metabolic stress attune to altered redox homeostasis. Bortezomib-induced proteasomal inhibition caused severe hepatocellular injury independent of ER stress via proapoptotic Apoptosis Signal-regulating Kinase 1 (ASK1)- c-Jun N-terminal kinase (JNK1)- p38 signaling concomitant with inadequate peroxisome proliferator-activated receptor γ (PPARγ)- Nuclear factor erythroid 2-related factor 2 (Nrf2) -driven antioxidant response. Although inhibition of ASK1 rescued acute hepatotoxicity, hepatic depletion of PPARγ or its physiological activator pigment epithelium-derived factor (PEDF) further aggravated liver injury even under ASK1 inhibition, emphasizing that endogenous PPARγ driven antioxidant activity serves as a prerequisite for the favorable therapeutic outcome of ASK1 inhibition. Consequently, ASK1 inhibitor selonsertib and PPARγ agonist pioglitazone in pharmacological synergism ameliorated bortezomib-induced hepatotoxicity and significantly prolonged survival duration in mice. Moreover, we showed that proteasome dysfunction is associated with ASK1 activation and insufficient PPARγ/Nrf2-driven antioxidative response in a subset of human nonalcoholic steatohepatitis (NASH) patients and the preclinical NASH model. The latter remains highly responsive to the drug combination marked by revamped proteasomal activity and alleviated hallmarks of NASH such as steatosis, fibrosis, and hepatocellular death. We thus uncovered a pharmacologically amenable interdependent binodal molecular circuit underlying hepatic proteasomal dysfunction and associated oxidative injury.

1. Introduction

Deregulation of protein homeostasis and proteotoxicity due to altered autophagic flux and proteasomal dysfunction are critical pathogenetic links in multiple aging-associated disorders including chronic liver diseases [1–3]. Of them, nonalcoholic fatty liver disease (NAFLD) is characterized by ER stress, altered autophagy, hepatocellular death, and marked accumulation of ubiquitinylated inclusion bodies [4–6]. Proteasomal dysfunction has also been implicated under ER stress, insulin resistance, and metabolism-associated inflammation [7]. Thus hepatic proteasomal dysfunction in the background of steatosis underscores the importance of proteotoxicity in the pathogenesis of NAFL and NASH.

Proteasomal inhibitors such as bortezomib, ixazomib, and carfilzomib are established chemotherapies used in multiple myeloma and mantle cell lymphoma patients with tolerable toxicity [8,9]. The efficacy of proteasomal inhibition is dependent on the sensitivity to the deregulation of protein-degradation systems as in the antibody-producing plasma cells. Similarly, being the major source of plasma proteins and
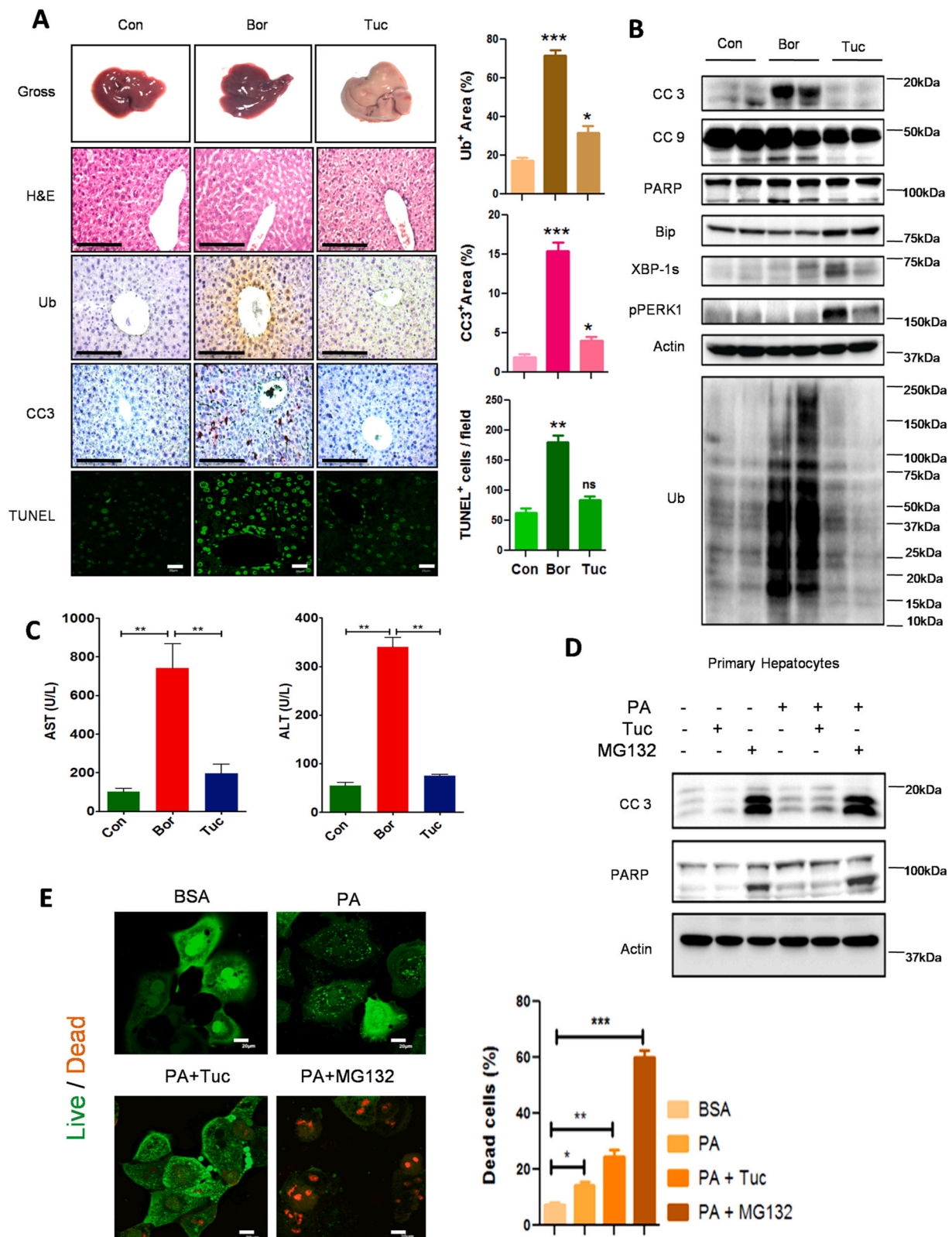
Fig. 1. Proteasomal inhibition induces severe hepatocellular injury than ER stress. (A–C) C57BL/6 mice were injected intraperitoneally with the vehicle, bortezomib (5 mg/kg), and tunicamycin (1 mg/kg) for 16 h (n = 3/group). (A) [left panels] Gross liver and liver sections stained for H&E, ubiquitin, cleaved caspase 3, and TUNEL positive cells; [right panels] Ubiquitin (brown), cleaved caspase 3 (magenta), and TUNEL positive cells (green) quantified (n = 3/group, 5 fields/sample). (B) Immunoblot for apoptosis markers (cleaved caspase 3, caspase 9, and PARP), ER stress markers (BiP, Xbp-1, and p-PERK1), and ubiquitin (Ub). (C) Serum AST and ALT levels. (D–E) Primary hepatocytes treated with Tunicamycin (Tuc, 5 μM) and MG132 (5 μM) both in the presence and absence of Palmitate (PA, 200 μM) for 16 h. Cells were analyzed by immunoblot (D) and Live-Dead assay by confocal microscopy (E). Percent dead cells for respective treatment groups (right panel; n = 5 fields/group). Values were presented as mean ± SEM, *P < 0.05; **P < 0.01; ***P < 0.001; ns, not significant. Scale bars, 100 μm (Histology); 20 μm (TUNEL, Live-Dead). (For interpretation of the references to color in this figure legend, the reader is referred to the Web version of this article.)
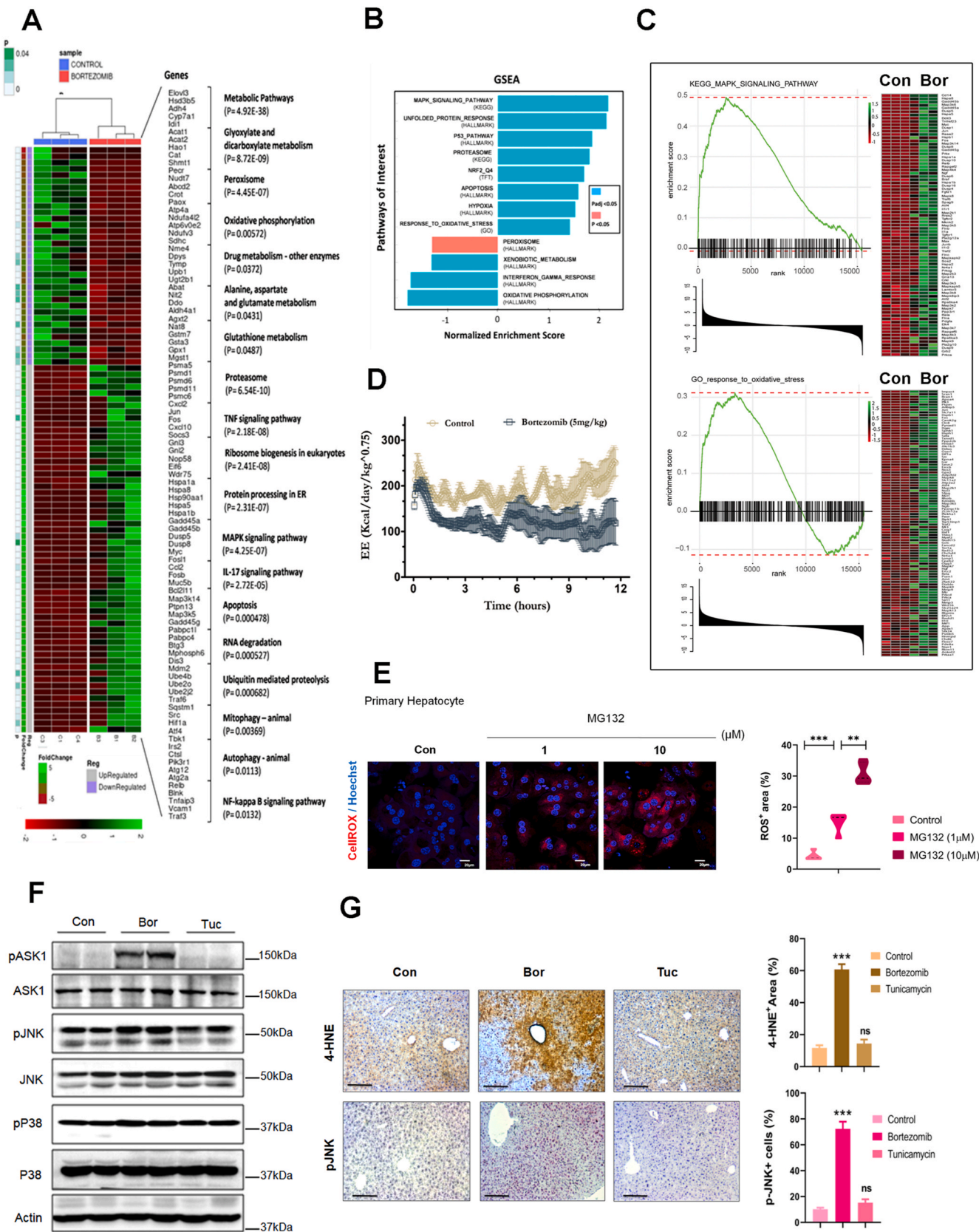
(caption on next page)

Fig. 2. Transcriptome-wide molecular pathway alterations in the liver under acute proteasomal inhibition. (A) Heatmap and partial list of differentially expressed genes identified from the RNA-Seq of vehicle and bortezomib (5 mg/kg) treated mice livers (n = 3/group). Enriched gene sets with top 5 enriched genes identified by KEGG pathway analysis shown with fold change and p values for enriched pathways. (B) GSEA from different pathway databases. Significantly enriched relevant gene sets were represented in the summary plot with normalized enrichment scores. Blue bar (Padj<0.05), Red bar (P < 0.05) (C) GSEA plot showing the heatmap of leading-edge genes for the GO_Response_to_oxidative_stress and KEGG_MAPK_signaling_pathway associated with proteasome inhibition. (D) Normalized Energy Expenditure (Kcal/day/kg$^{0.75}$) calculated for 12 h (light cycle) in vehicle and bortezomib treated groups (n = 3/group). (E) [Left panel] Primary hepatocytes were treated with MG132 for 16 h and analyzed using confocal microscopy for ROS generation. Cell nucleus was counterstained with Hoechst 33,342; [Right panel] Percent ROS$^+$ area (Deep red) were calculated using the color threshold function (n = 5 fields/group). (F) Immunoblot assays were performed with the liver lysates of vehicle, bortezomib, and tunicamycin treated mice for assessing ASK1 signaling cascade (pASK1, pJNK, and pP38); (n = 3/group). (G) Immunohistochemistry for 4-HNE (Brown) and p-JNK (magenta) were performed [left panel] and quantified [right panel] (n = 3/group, 5 fields/sample). Values were presented as mean ± SEM, *P < 0.05; **P < 0.01; ***P < 0.001; ns, not significant. Scale bars, 100 μm (IHC) 20 μm (confocal). (For interpretation of the references to color in this figure legend, the reader is referred to the Web version of this article.)

lipoproteins, hepatocytes would also be susceptible to proteasomal inhibitor-dependent cytotoxicity. Indeed, cases of bortezomib-induced hepatitis and fatal liver failure have already been reported in patients with multiple myeloma [10–12].

Alteration of ubiquitin homeostasis with the accumulation of both polyubiquitylated conjugates and free ubiquitin designated as ubiquitin stress [13]. Dysregulated proteostasis due to proteasomal inhibition or dysfunction serves as a cellular stressor leading to the activation of various adaptive stress responses including macroautophagy, proteaphagy, the formation of ubiquitylated inclusion bodies, and proteasome biogenesis [14–16]. Insufficient or inappropriate stress response may conversely activate the apoptosis pathway conferring the adverse outcome of proteasomal inhibition [17–19]. Mechanistically, proteasomal inhibitors such as MG132 and bortezomib have been shown to cause apoptosis in various cell types through the generation of reactive oxygen species (ROS) [20–24]. However, the molecular basis for ROS-induced apoptosis and its reversal thereof in the context of acute or chronic proteotoxicity is still elusive.

Here we have shown that acute inhibition of proteasomal activity leads to profound hepatic injury and dysfunction, effects that are associated with ROS accumulation that in turn promotes ASK1-JNK1 dependent hepatocellular death with concomitant failure in surmounting an effective anti-oxidant response through PEDF-PPARγ-Nrf pathway. Proteasomal dysfunctions concomitant with analogous deregulation of these pathways are also observed in human and murine NASH. Interestingly, co-treatment with ASK1 inhibitor and PPARγ activator potently reverses hepatic proteotoxicity and extends survival in acute proteasome inhibition, and alleviates NASH in mice.

2. Material and methods

2.1. Animal model

All experiments were approved by the Institutional Animal Ethics Committee at the CSIR-Indian Institute of Chemical Biology, approved by the Committee for Control and Supervision of Experiments on Animals (CPCSEA), Ministry of Environment and Forest, and Government of India. 6–8 weeks old C57BL/6 male mice were housed in a 12 h light/dark cycle at 22±1 °C with free access to food and water. Mice were fed a 60% high-fat diet (HFD)[Protein 20%, Fat 60%, Carbohydrate 20% and Energy Density 5.21% Kcal/g] (D12492, Research Diets, New Brunswick, USA) for 16 weeks. Mice were gavaged daily by vehicle (DMSO in 0.9% saline), Selonsertib (SelleckChem, Houston, USA; 10 mg/kg), Pioglitazone (Sigma-Aldrich, Missouri, USA; 30 mg/kg), Selonsertib, and Pioglitazone for the last 4 weeks with ad libitum fed HFD-diet and water. For the survival experiment, mice were injected with Bortezomib (2.5 mg/kg) in 0.9% saline intraperitoneally every 24 h. Animals were randomized into four treatment groups and the drugs were administered by gavage 4 h before Bortezomib treatment. Survival was assessed 6 hourly for 72 h.

2.2. Adenovirus and adeno-associated virus (AAV)

Adenoviruses containing short-hairpin (sh) RNA targeting PEDF (Ad-shPEDF-#1), PPARγ (Ad-sh PPARγ-#1), and EGFP (Ad-shEGFP) were generated with BLOCK-iT Adenoviral RNAi Expression System (Invitrogen). The shRNA sequences are following: Ad-shPEDF-#1: 5'-GGAGCTCCTTGCCTCTGTTACGTAACAGAGGCAAGGAGCTCC-3'; Ad-sh PPARγ-#1: 5'- GCCCTTTACCACAGTTGATTTAAATCAACTGTGGTAAAG GC-3'. Adenoviruses were purified (PureVirus™ Adenovirus Purification Kit, CELL BIOLABS INC.) and administered 2.5X 10^{12} pfu/mice through tail vein injection. AAV for the overexpression of LacZ and PEDF were generated with AAV Helper-Free System (Agilent, California, USA).

2.3. Glucose- and insulin tolerance test (OGTT, IP ITT)

OGTT and ITT were performed as previously described by Mouse Metabolic Phenotyping Centers (MMPC). For the OGTT, Mice were fasted for 12 h and fed with glucose 2 g/kg whereas, for ITT, 0.5 IU/kg of body weight insulin (Actrapid, Novo Nordisk, India) was intraperitoneally injected after 6 h fasting. Fasting Blood glucose levels were detected from the tail-tip cut with a glucometer (Accu-Check Aviva).

2.4. Liver enzyme

Blood was collected by cardiac puncture from anesthetized mice and serum alanine aminotransferase (ALT) and aspartate aminotransferase (AST) levels were determined using the kinetic method by commercially available kit (Randox Laboratories).

2.5. Histology, Picro Sirius red staining (PSR), and immunohistochemistry (IHC)

Paraffin-embedded liver tissue sections (5 μm thick) were deparaffinized in xylene and rehydrated and processed for hematoxylin and eosin and PSR (1.2% w/v; Direct red-80 Sigma-Aldrich) staining. Images were taken using an inverted light microscope (Zeiss Axiovert CFL 40 Trinocular Inverted Fluorescence Microscope). For IHC, tissue sections were baked at 80 °C for 15 min and rehydrated. Antigen retrieval was done by heating in the microwave with sodium citrate buffer (10 mM sodium citrate, 0.05% Tween 20, pH-6.0). Two different kits used for immunohistochemical staining; VECTASTAIN ABC KIT (Biotinylated Horseradish Peroxidase Anti-rabbit IgG) and ImmPRESS Duet Double staining Polymer kit (Horseradish Peroxidase Anti-Mouse IgG/Alkaline Phosphatase Anti-Rabbit IgG).

2.6. Terminal deoxynucleotidyl transferase dUTP nick end labeling (TUNEL) assay

Tunel assay was performed using Click-iT® TUNEL Alexa Fluor® Imaging Assay (Invitrogen) with Fluoromount Aqueous mounting Medium (Sigma) and Hoescht for counterstaining. Images were captured with the confocal microscope FluoView (FV10i; Olympus, Tokyo, Japan).
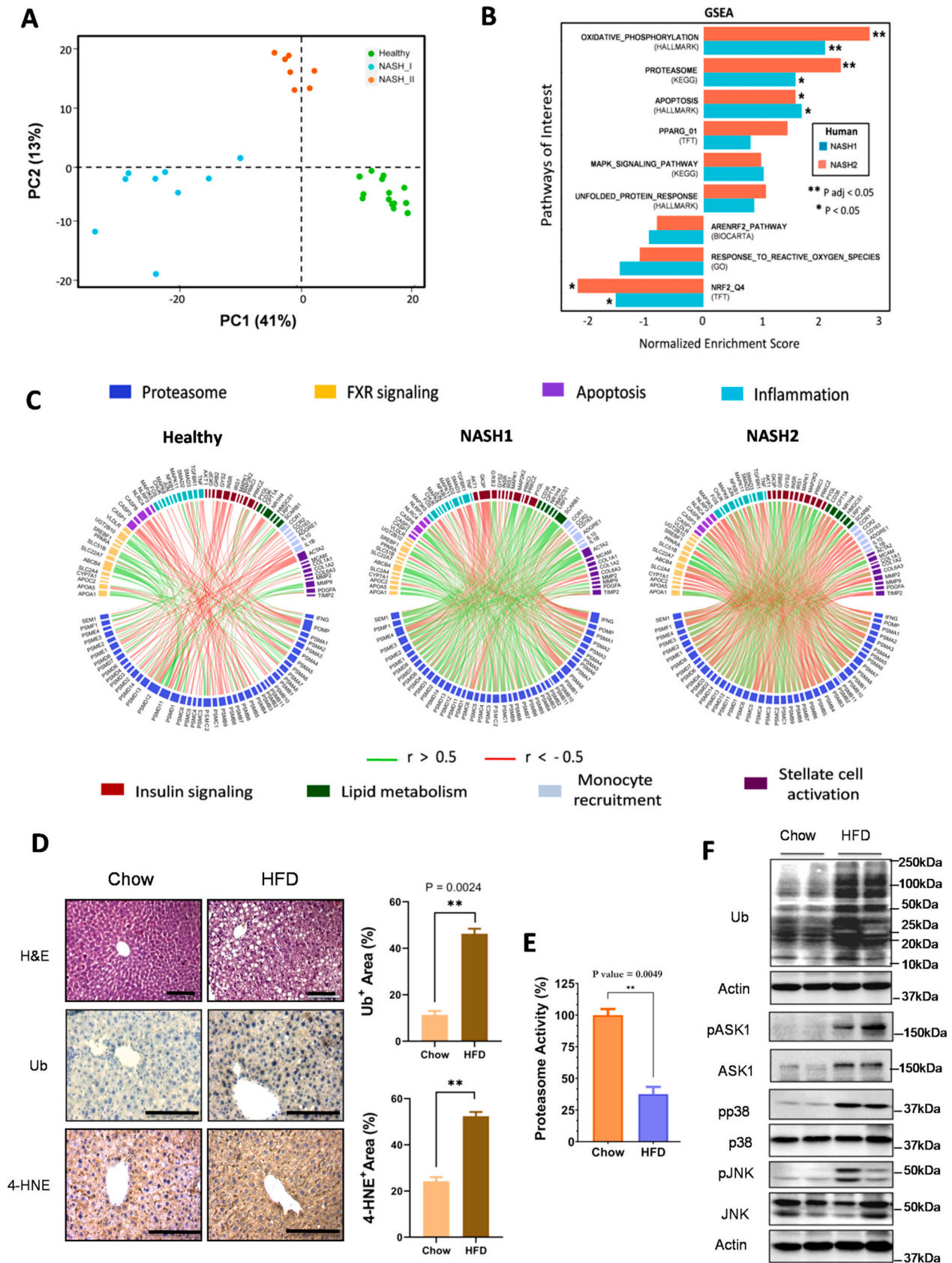
(caption on next page)

Fig. 3. Proteasome dysfunction is associated with ASK1 activation and anti-oxidative response in human NASH and preclinical NASH model. (A) PCA analysis of the liver transcriptome of healthy (n = 14) and NASH patients (n = 16) from a published dataset. (B) GSEA analysis was performed with both the NASH1 (n = 9) and NASH2 (n = 7) group independently for the targeted pathways associated with the hepatic proteasomal stress. Significantly enriched and depleted pathways were represented in the summary plot with their normalized enrichment score. (C) Circos plot illustrates the correlation between proteasomal genes and targeted list of NASH hallmark genes (FXR signaling, apoptosis, inflammation, insulin signaling, lipid metabolism, monocyte recruitment, and stellate cell activation) for healthy, NASH1, and NASH2 groups based on the correlation coefficients among gene expressions; green chords (r > 0.5), red chords (r < −0.5). (D) Mice were fed with a chow diet and HFD for 16 weeks (n = 4). H&E along with the immunohistochemistry for Ubiquitin and 4-HNE was performed and positive areas (%) were quantified (bottom panel; n = 4/group, 5 fields/sample). (E) Chymotrypsin-like proteasomal activity (%) was quantified from chow and HFD-fed mice liver lysates (n = 4). (F) Immunoblot assays for ASK1 activity markers (p-ASK1, p-JNK, p-p38) and ubiquitin (Ub). Values were presented as mean ± SEM, **P < 0.01; Scale bars, 100 μm (Histology); 20 μm (Immunohistochemistry). (For interpretation of the references to color in this figure legend, the reader is referred to the Web version of this article.)

2.7. Metabolic cage

Mice were housed in metabolic cages (LE 405 Gas Analyzer; Panlab, Harvard Apparatus) and allowed to acclimatize 24 h before the experiment, and VO2, VCO2, energy expenditure, and respiratory quotient data collected over 12 h.

2.8. Immunoblotting

Proteins extracted from cells or tissue by lysis buffer (50 mM Tris-HCl (pH 7.4), 100 mM NaCl, 1 mM ethylenediaminetetraacetic acid (EDTA), 1 mM ethylene glycol-bis(β-aminoethyl ether)-N,N,N′,N'-tetraacetic acid (EGTA), and 1% Triton X-100 along with protease- and phosphatase inhibitor cocktail (Roche) were resolved by sodium dodecyl sulfate-polyacrylamide gel electrophoresis (SDS-PAGE), transferred to polyvinylidene fluoride (PVDF) membrane (Immobilon-P, Merck Life Sciences), incubated overnight with primary antibody followed by incubation with peroxidase-conjugated secondary antibodies and bands were visualized with a ChemiDoc MP Imaging System (Bio-Rad, Hercules, CA, USA).

2.9. Live dead and caspase 3/7 activity assay

Cells were stained using LIVE/DEAD®Viability/Cytotoxicity Kit for mammalian cells (Invitrogen). Caspase 3/7 activity was assessed using 4 μM CellEvent™ Caspase-3/7 Green Detection Reagent (Invitrogen). Cells were imaged using the confocal microscope FluoView (FV10i; Olympus, Tokyo, Japan).

2.10. Oxidative stress measurement

Cells were incubated with the 5 μM CellRox Deep Red Reagent (Invitrogen) at 37 °C for 30 min and Hoescht for 20 min, washed and imaged using a confocal microscope at excitation/emission maxima for the reagent 644/665 nm.

2.11. RNA interference (RNAi)

shRNA plasmids, including a non-target control (#TR30013) and several shRNA targeting ASK1 (FI37885, #FI37886, #FI37887, #FI37888; Origene) were transfected using Lipofectamine 2000 (Invitrogen). ASK1 knockdown was confirmed by Western blotting.

2.12. Hepatocyte culture

Primary hepatocytes were isolated from mice weeks according to the protocol previously described [25] and maintained in Hepatozyme (gibco® Life technologies™, Paisley, UK) supplemented with L-glutamine, 1% penicillin-streptomycin. Hepatocytes were then infected for 48 or 72 h with adenoviruses at MOI of 40. Human hepatoma cell line HepG2 was cultured in Minimum Essential Medium (HIMEDIA, Maharashtra, India) supplemented with 10% FBS and 1% Penicillin-Streptomycin.

2.13. Subcellular fractionation

Trypsinized primary hepatocytes were harvested in ice-cold PBS and centrifuged at 100g at 4 °C for 10 min to pellet the cells. The pellet was resuspended in Buffer 1 (150 mM NaCl, 50 mM HEPES, 25 μg/ml digitonin (Calbiochem), pH-7.4, protease and phosphatase inhibitor (Roche) and incubated in ice for 10 min following which it was centrifuged at 2000 g at 4 °C for 10 min to obtain the cytosolic and membrane protein in the supernatant. The pellet was then washed with ice-cold PBS at 100g at 4 °C for 10 min, resuspended by vortexing in Buffer 2 (150 mM NaCl, 50 mM HEPES, 1% NP-40, pH-7.4, protease, and phosphatase inhibitor), incubated in ice for 30 min, and centrifuged at 7000g at 4 °C for 10 min to obtain the mitochondrial fraction in the supernatant and pellet down the nuclei and cellular debris. The pellet was resuspended in Buffer 3 (150 mM NaCl, 50 mM HEPES, 0.1% SDS, pH-7.4, protease, and phosphatase inhibitor) and vortexed periodically for 30 min. Following this, the suspension was incubated in ice for 1 h and then centrifuged at 7000g at 4 °C for 10 min to obtain the nuclear protein in the supernatant.

## 2.14. Proteasome activity assay

Proteasome activity was assayed in homogenized freshly isolated liver tissue following three cycles of freezing and thawing in chymotrypsin-like activity in assay buffer containing 100 mmol/L Tris-HCl (pH 8.0), 2 mmol/L ATP, and fluorogenic peptide substrate (0.1 mmol/L) according to a procedure previously described [7].

2.15. Isobologram analysis

HepG2 cells seeded in a 96-well plate were pre-treated with multiple doses of TCASK10 (Tocris) or Rosiglitazone (Sigma) or their combination following which MG132 (10 μM) was administered. After 16h, cell death was detected by LIVE/DEAD®Viability/Cytotoxicity Kit (Invitrogen) and fluorescence was measured with BioTek Synergy H1 Hybrid Reader (Vermont, USA). Multiple drug-effect analysis of Chou-Talalay based on the median-effect principle was used [26] and the combination index for synergism or antagonism or additive effect was calculated as described by Chou [27].

2.16. Antibodies

Antibodies against ASK1(#8662), phospho-ASK1 (#3765), p38 MAP kinase (#8690), phospho- p38 MAP kinase (#4511), JNK (#9252), phospho-JNK (#4668), Poly (ADP-ribose) polymerase (PARP) (#9542), Cleaved Caspase-3 (CC3) (#9661), Caspase 9 (C9) (#9508), NRF2 (#12721), PPARγ (#2435), phospho- PERK (#3179), X-box binding protein 1(XBP1) (#83418), Binding immunoglobulin protein (BIP) (#3183), Ubiquitin (#3933), Histone H3 (#4499) and MYC-TAG (#2278) were purchased from Cell Signaling Technology (Beverly, USA). Anti-PEDF was from Millipore (Massachusetts, USA) and 4-Hydroxynoneal (4-HNE) was from R&D Systems (MAB3249, Minneapolis, USA). β-actin (#A2228) and α-tubulin (#T6199) antibodies were purchased from Sigma-Aldrich (St. Louis, Missouri, United States)
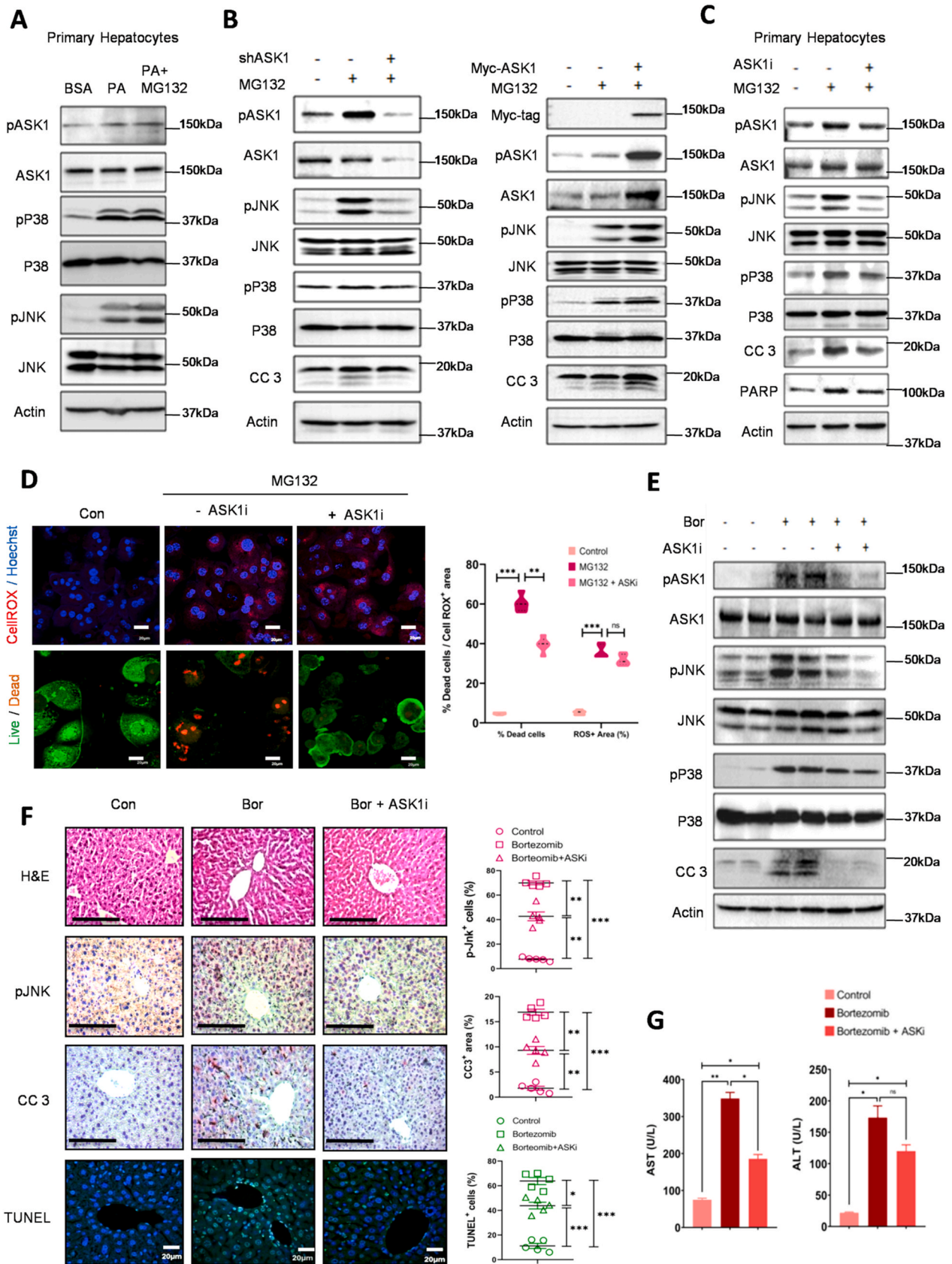
(caption on next page)

Fig. 4. ASK1 activation promotes ROS-driven proteotoxic liver injury. (A) Primary hepatocytes treated with palmitate (200 μM) both in the presence and absence of MG132 (10 μM) for 12 h and probed for ASK1 activation. (B) HepG2 cells were treated with MG132 (10 μM) both in ASK1 knockdown (sh-ASK1) (left panels) and ASK1 overexpressed (myc-ASK1) (right panels) cells for 12 h. Immunoblot assays were performed for ASK1 activation and cleaved caspase 3. Total ASK1, JNK, P38, and Actin were taken as the loading control. (C–D) Primary hepatocytes treated with MG132 (10 μM) for12h in the presence and absence of TCASK10 (ASKi, 30 μM). ASK1 activation (p-ASK1, p-JNK, and p-p38) and apoptosis (cleaved caspase 3 and PARP) were determined by immunoblots (C). Apoptosis (Live-Dead assay) and ROS generation (CellROX) were assessed using confocal microscopy [left panel] and quantified [right panel] for Dead cells and ROS$^+$ area (%); n = 5 fields/group (D). (E–F) Mice were intraperitoneally injected with bortezomib (5 mg/kg) for 12 h in the presence and absence of Selonsertib (ASKi, 10 mg/kg), injected intra-peritoneally 4 h before the bortezomib treatment and in every 4 hours interval (n = 5/group). ASK1 activity and apoptosis were accessed by immunoblot (E) and Immunohistochemistry (F). Percent of p-JNK$^+$ cells (magenta) cleaved caspase 3$^+$ area (magenta) and TUNEL$^+$ cells (green) were quantified [right panel] (n = 5/group, 5 fields/sample). (G) Serum AST and ALT levels were measured for three groups. Values were presented as mean ± SEM, *$P < 0.05$; **$P < 0.01$; ***$P < 0.001$; ns, not significant. Scale bars, 100 μm (Histology); 20 μm (TUNEL, Live-Dead, and CellROX). (For interpretation of the references to color in this figure legend, the reader is referred to the Web version of this article.)

2.17. Human and mice transcriptomics analysis

Mouse livers in triplicate (C1, C3, and C4 control, B1, B2, and B3 are bortezomib) were used for transcriptomic analysis. A modified NEBNext RNA Ultra II directional protocol is used to prepare the libraries for total RNA. Libraries were sequenced on Illumina HiSeqXTen to generate 50 M, 2x150bp reads/sample. The fastq samples were mapped to *Mus musculus* GRCm38 genome using STAR (v2.27.2b) to create bam files [28] and further processed using Rsamtools, Rsubread, and GenomicAlignments R packages to create the abundance table [29]. The count table was then normalized and differentially abundant genes were identified using the DESeq2 R package [30]. Genes with a change greater than two folds with p-value< 0.05 and adjusted p-value< 0.05 were considered significant. Gene set enrichment analysis (GSEA) was performed using the fgsea R package and the mouse version of MSigDB [31]. Also, for all heatmaps of transcripts, counts per million normalizations were performed from raw counts using the edgeR package and visualization was performed using pheatmap function [32]. For reanalysis of a previously sequenced human dataset [33] samples were processed similar to as mentioned previously using the *Homo sapien* GRCm38 genome for alignment and MSigDB gene-sets for GSEA [34].

2.18. Statistics

Data were represented as mean ± SEM and Graphpad Prism 8 software was used for statistical analysis. T-test and ANOVA were used as appropriate followed by Bonferroni post-hoc test. $P < 0.05$ was considered statistically significant. Two-tailed Fisher's Exact Test was performed for contingency table analysis to compute the exact P-value.

3. Results

3.1. Proteasomal inhibition but not ER stress induces hepatocellular injury

To determine whether proteasomal inhibition and ER stress could independently cause hepatic injury, we observed, tunicamycin treatment led to marked lipid accumulation with a modest increase in TUNEL and CC3 positive cells while bortezomib caused striking sinusoidal dilatation, pericentral ubiquitin accumulation, and a significant increase in the number of TUNEL and CC3 positive cells (Fig. 1A). Conspicuous liver injury following bortezomib and not tunicamycin injection was also shown by immunoblot for CC3, Cleaved Caspase 9 (CC9), and cleavage of PARP. Conversely, tunicamycin treatment increased ER stress markers such as Bip, XBP-1, and phospho-PERK1 which were remained unaltered by bortezomib (Fig. 1B). Serum ALT and AST levels, two established markers of liver injury also followed a similar pattern following bortezomib administration (Fig. 1C). Immunoblotting and live-dead assays revealed that MG132 treatment resulted in significant hepatocyte apoptosis when compared to palmitate and tunicamycin (Fig. 1D-E), suggesting cell-autonomous effects of proteasomal inhibition. Thus, we confer that proteasomal inhibition causes significant hepatotoxicity independent of the ER stress pathway.

3.2. Proteasomal inhibition registers a transcriptional program for oxidative stress response and MAPK signaling in liver

Transcriptomics analysis from control and bortezomib treated mice livers (Supplementary Fig. 1A) revealed a total of 4663 differentially expressed genes (DEGs) with about 54% (n = 2499) and 46% (n = 2164) were respectively up-and down-regulated. Pathway analysis (KEGG) of DEGs revealed bortezomib-induced proteasomal inhibition resulted in the significant (FDR <0.05) upregulation of proteasomal genes, mitogen-activated protein kinase (MAPK) signaling pathway, and apoptosis suggesting proteotoxic hepatocellular injury, whereas significant (FDR <0.05) downregulation of peroxisome and oxidative phosphorylation genes suggesting mitochondrial damage and inadequate anti-oxidative response (Fig. 2A, Supplementary Fig. 1B) accompanied by overall suppression of metabolic pathway genes. GSEA further confirmed significant depletion (Padj<0.05) of several metabolic pathways including oxidative phosphorylation, peroxisomal oxidation, and xenobiotic-metabolism with the concomitant enrichment (Padj<0.05) of the genes associated with MAPK signaling cascade, unfolded protein response, p53 pathway, apoptosis, hypoxia, and ROS-mediated response (Fig. 2 B, C and Supplementary Fig. 2).

Bortezomib treatment in mice caused a significant drop in energy expenditure, oxygen consumption, and carbon dioxide release without an altered respiratory quotient (Fig. 2D and Supplementary Fig. 3 A-C) indicating overall metabolic suppression as evident by metabolic cage analysis. MG132 treatment further revealed a dose-dependent ROS production that resulted in hepatocellular death (Fig. 2E and Supplementary Fig. 3D), supporting pan-transcriptomic oxidative-stress response. Autophosphorylation and activation of ASK1 are regulated by the ROS-mediated uncoupling with reversible oxidation of redox-regulated partner thioredoxin [35]. Following activation, ASK1 selectively phosphorylates its downstream kinases JNK1 and p38 which lead to hepatocyte apoptosis [36,37]. Even, ASK1 inhibitor, selonsertib, has been implicated in clinical trials for NASH therapy [38,39]. We thereby examined whether proteasomal blockade could activate ASK1 and promote liver injury. As shown in Fig. 2F and Supplementary Fig. 3E, bortezomib and not tunicamycin specifically induce ASK1 phosphorylation and its downstream targets JNK1 and p38. IHC of bortezomib and not tunicamycin treated liver also revealed enhanced JNK1 phosphorylation and accumulation of 4-HNE, a lipid peroxidation product and a marker of oxidative stress (Fig. 2G and Supplementary Fig. 3F).

3.3. Proteasomal dysfunctions in human and murine NASH are associated with ASK1 activation and oxidative stress response

To examine the contributions of hepatic proteasomal dysfunction in metabolic syndrome, we analyzed the transcriptome of healthy (n = 15) and NASH (n = 16) livers [33]. Principal Component Analysis (PCA) revealed two independent sample clusters within the NASH group which were empirically labeled as NASH1 and NASH2 (Fig. 3A). GSEA analysis revealed a significant enrichment of proteasome (P adj<0.05) and apoptosis pathway in concordant with depletion of NRF2 target genes (P < 0.05) (Fig. 3B). Association study showed a gradual increase in the
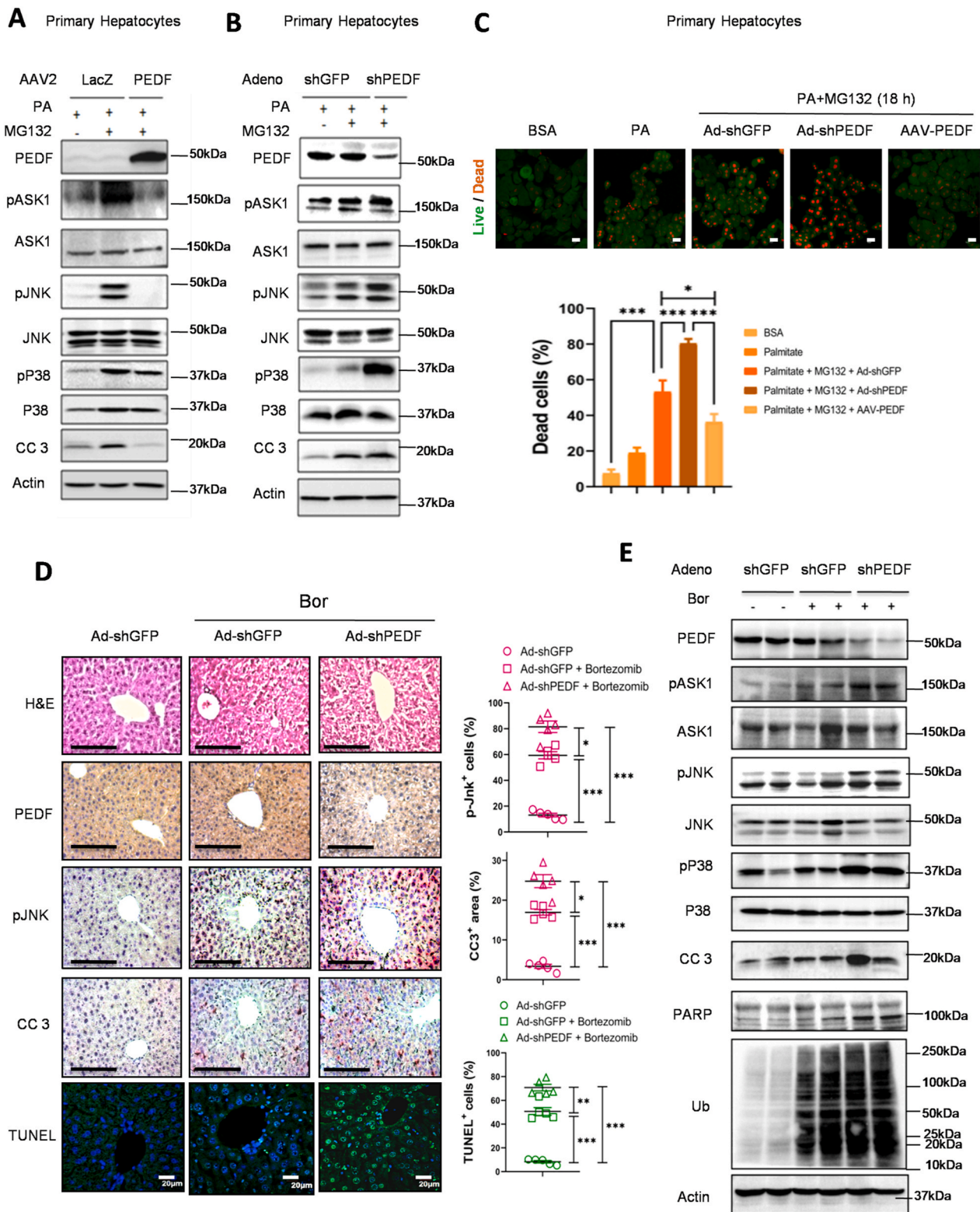
Fig. 5. PEDF dampens proteotoxic hepatocellular death by inhibiting ASK1. (A–C) PEDF was knockdown and overexpressed in primary hepatocytes by transducing with AAV2-PEDF (A) and Ad-shPEDF (B) and cells were treated with MG132 (10 μM) for 16 h and analyzed for ASK1 activation and apoptosis using immunoblots and Live-Dead assay using confocal microscopy (C). Ad-shGFP and AAV2-LacZ were used as mock. Percent of Dead cells (orange) were further quantified using [bottom panel] (n = 5 fields/sample). (D–E) Mice were intravenously injected with Ad-shPEDF; after 7days, mice were intraperitoneally administered with bortezomib (5 mg/kg) for 16h (n = 5/group). Ad-shGFP was used as a mock and DMSO was treated as a vehicle. PEDF knockdown efficiency, ASK1 activation, and apoptosis were assessed by immunohistochemistry (D) and immunoblot assays (E). Percent of p-JNK^{+} cells (magenta) cleaved caspase 3[+] area (magenta) and TUNEL^{+} cells (green) were quantified [D; right panel] (n = 5/group, 5 fields/sample). Values were presented as mean ± SEM, *P < 0.05; **P < 0.01; ***P < 0.001. Scale bars, 100 μm (Histology); 20 μm (TUNEL and Live-Dead). (For interpretation of the references to color in this figure legend, the reader is referred to the Web version of this article.)
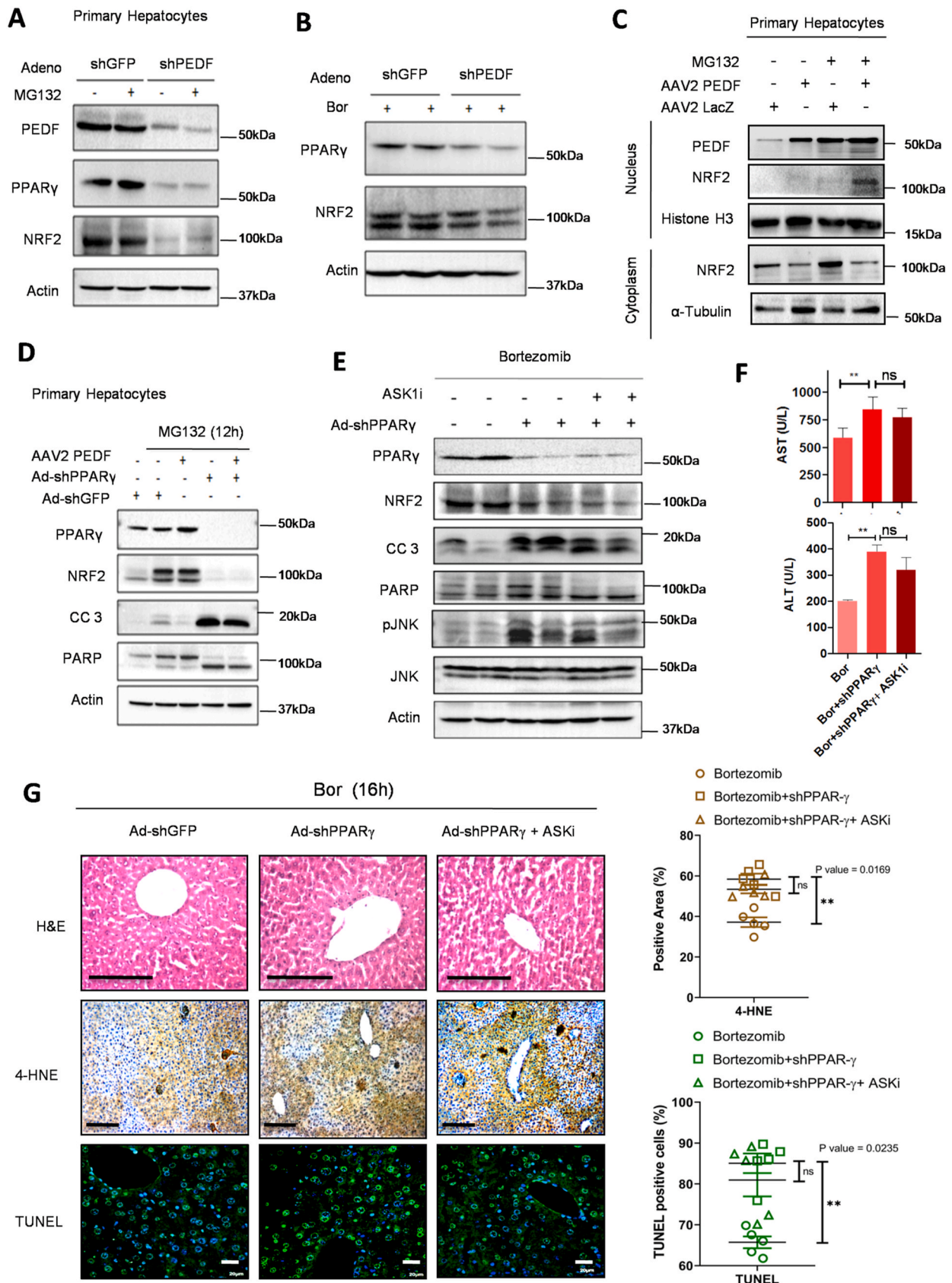
(caption on next page)

Fig. 6. PPARγ governs the anti-oxidative property of PEDF in proteotoxic liver damage. (A) Primary hepatocytes were transduced with Ad-shPEDF, treated with MG132 (10 μM) for 12h, and analyzed for PEDF, PPARγ, and Nrf2 expressions. (B) C57BL/6 mice were injected with Ad-shPEDF and administered with bortezomib (5 mg/kg) after 7 d (n = 5/group). Immunoblot blot assay was performed to assess the expression of PPARγ and Nrf2. (C) Primary hepatocytes were transduced with AAV2-PEDF followed by the treatment with MG132 (10 μM) for 8h, nuclear and cytosolic fractions were collected and expressions of PEDF, Nrf2 were assayed by immunoblot; Histone H3 and α-tubulin were used as nuclear and cytosolic markers respectively. (D) PPARγ was knocked down and PEDF was concomitantly overexpressed in primary hepatocytes by transducing with Ad-shPPARγ and AAV2-PEDF. MG132 (10 μM) were treated for 12h and expressions of PPARγ, Nrf2, Cleaved caspase 3, and PARP were determined. (E–G) PPARγ was knocked down in mice liver by injecting Ad-shPPARγ. After 7d of adenoviral infection, mice were administered with a single dose of bortezomib (5 mg/kg) in the presence and absence of Selonsertib (ASKi, 10 mg/kg) given once 4 h before the and twice after the bortezomib treatment; (n = 5/group). (D) Expression of PPARγ, Nrf2, Cleaved caspase 3, PARP, p-JNK, and JNK was assayed by immunoblot. (E) Serum AST and ALT levels. (F) [left panel] ROS generation and cellular death were assessed using immunohistochemistry of 4-HNE and TUNEL assay. [right panel] Quantification of percent 4-HNE positive area (brown) and TUNEL positive cells (green) (n = 5/group, 5 fields/sample). Values were presented as mean ± SEM, *P < 0.05; **P < 0.01; ***P < 0.001; ns, not significant. Scale bars, 100 μm (Histology); 20 μm (TUNEL). (For interpretation of the references to color in this figure legend, the reader is referred to the Web version of this article.)

number of correlations ($-0.5 > \rho > 0.5$) between the subset of genes related to the proteasome, JNK activation, and ARENRF2 pathway among healthy, NASH1, and NASH2 groups (Supplementary Fig. 4A). Precisely, in the NASH2 group, we observed a significant gain in negative correlations (NASH1/NASH2; 56/104) between the genes associated with the activation of JNK and ARENRF2 pathway (p < 0.0001). Conversely, proteasomal genes predominantly gained positive correlations (p < 0.0001) with the geneset of both JNK activation (NASH1/NASH2; 154/234) and ARENRF2 pathway (NASH1/NASH2; 72/130) (Supplementary Fig. 4B). We next asked if expressions of proteasomal genes are associated with the NASH signature genes including a subset of the DEGs such as FXR signaling, apoptosis, insulin signaling, lipid metabolism, inflammation, monocyte recruitment, and hepatic stellate cell activation [33]. In NASH patients, proteasomal genes showed a significant increase in the number of correlations ($-0.5 > \rho > 0.5$) with the NASH signature genes. Moreover, the NASH2 group exhibits the highest number of correlations (positive/negative, 399/619) between the proteasomal genes and NASH specific genes, followed by NASH1 (positive/negative, 297/193) and healthy group (positive/negative, 58/99) (Fig. 3C). Thus, similar to drug-induced proteasomal inhibition our analysis reveals that overt proteasomal dysfunction in human NASH is not only associated with JNK activation and NRF2 mediated anti-oxidative response but correlated with alterations of NASH hallmark genes.

Taking cues from the human transcriptomics data we next sought to validate these findings in the preclinical NASH model. Mice fed with HFD for sixteen weeks showed hepatomegaly with expanded adipose mass and developed hallmarks of NASH including steatosis, fibrosis showed by Sirius red staining, HSC activation revealed by immunohistochemistry of alpha-smooth muscle actin, and elevated serum AST and ALT levels (Supplementary Figs. 5A–C). Interestingly, we find a marked presence of ubiquitylated proteins, as well as 4-HNE in HFD-fed mice liver sections (Fig. 3D), and a significant drop in proteasomal activity (Fig. 3E). Moreover, immunoblots of the liver also revealed the accumulation of polyubiquitylated proteins and the activation of ASK1, JNK1, p38 pathways (Fig. 3F). Thus HFD induced NASH mimics proteasomal dysfunction in terms of accumulation of polyubiquitylated proteins and oxidative stress.

3.4. ASK1 mediates proteotoxic liver injury

We next examined whether ASK1 activation is necessary for proteotoxicity in a hepatocyte autonomous manner. Similar to in-vivo results, primary hepatocytes treated with palmitate and MG132 activate the ASK1-JNK1-p38 pathway (Fig. 4A). Knockdown of ASK1 by shRNA in HepG2 cells suppressed while overexpression of myc-tagged ASK1 augments JNK1 and p38 phosphorylation with corroborating levels of CC3, suggesting the crucial role of ASK1 activation in proteotoxic cellular death (Fig. 4B and Supplementary Fig. 6A). Primary hepatocytes treated with selective ASK1 inhibitor TCASK10 potently attenuated MG132 induced apoptosis, however without affecting cellular ROS levels (Fig. 4C and D and Supplementary Fig. 6B). Oral gavage with

selonsertib, a clinically approved ASK1 inhibitor robustly blocked bortezomib-induced activation of ASK1-JNK1 pathway as well as apoptosis in mice liver (Fig. 4E and F and Supplementary Fig. 6C). Expectedly, serum AST and ALT levels were also significantly reduced by ASK1i (Fig. 4G). Taken together, ASK1 serves as a critical signaling node in hepatic injury under proteasomal stress.

3.5. PEDF protects from proteotoxic hepatic injury by inhibiting ASK1

PEDF has emerged as a potent hepatoprotective secretory glycoprotein with strong anti-oxidant properties [40,41]. Since disproportionate ROS production has been a major contributor to proteotoxic liver injury, we next sought to examine the impact of PEDF in this context. AAV2 mediated overexpression of PEDF remarkably suppressed MG132 dependent hepatocyte apoptosis, activation of ASK1, and ROS production (Fig. 5A, C and Supplementary Fig. 7A). Conversely, knockdown of PEDF using adenovirus carrying shRNA targeting PEDF, augmented proteotoxic apoptosis and enhanced ASK1 activation (Fig. 5B and C). Ectopic expression of PEDF also rendered ASK1 inhibitor dispensable for MG132 dependent apoptosis while ASK1 inhibitor could not reverse cell death in PEDF depleted condition (Supplementary Figs. 7B and C). To further determine the impact of PEDF expression on proteotoxic liver injury in vivo, hepatic PEDF was depleted by adenovirus (Fig. 5D and E and Supplementary Fig. 7D). Knockdown of PEDF enhanced bortezomib-induced ASK1 activation and apoptosis without affecting ubiquitylated protein accumulation (Fig. 5D and E).

3.6. PPARγ mediates protective effects of PEDF through the antioxidant program

In the search for a downstream mediator of hepatoprotective effects of PEDF in the context of oxidative stress, we examined the role PPARγ, a transcription factor was shown to be positively regulated by PEDF in various cells and tissues [42,43]. Moreover, PPARγ in a positive feedback loop with nuclear factor Nrf2 [44] constitutes a transcriptional program that plays a pivotal protective role in oxidative and xenobiotic stresses [45–48]. Knockdown of PEDF in primary hepatocytes leads to downregulation of both PPARγ and Nrf2 independent of MG132 treatment (Fig. 6A). Consistently, adenovirus-mediated depletion of PEDF in mice liver caused decreased PPARγ expression even under bortezomib treatment (Fig. 6B). Ectopic expression of PEDF in hepatocytes conversely leads to increased PPARγ and Nrf2 expressions. Moreover, AAV2 mediated overexpression of PEDF in primary hepatocytes resulted in nuclear translocation of Nrf2 under proteotoxic stress indicating PEDF mediated Nrf2-driven antioxidant response under proteasomal inhibition (Fig. 6C). However, the anti-apoptotic effects of PEDF were rendered ineffective when PPARγ was concomitantly knocked down (Fig. 6D). Moreover, this remarkable suppression of Nrf2 expression following adenovirus-mediated knockdown of PPARγ (Fig. 6D and Supplementary Fig. 8A) is suggestive of a functional PEDF-PPARγ-Nrf2 antioxidant signaling axis in the liver. Consistently, a specific PPARγ agonist rosiglitazone (Rosi) protects hepatocytes from apoptosis and
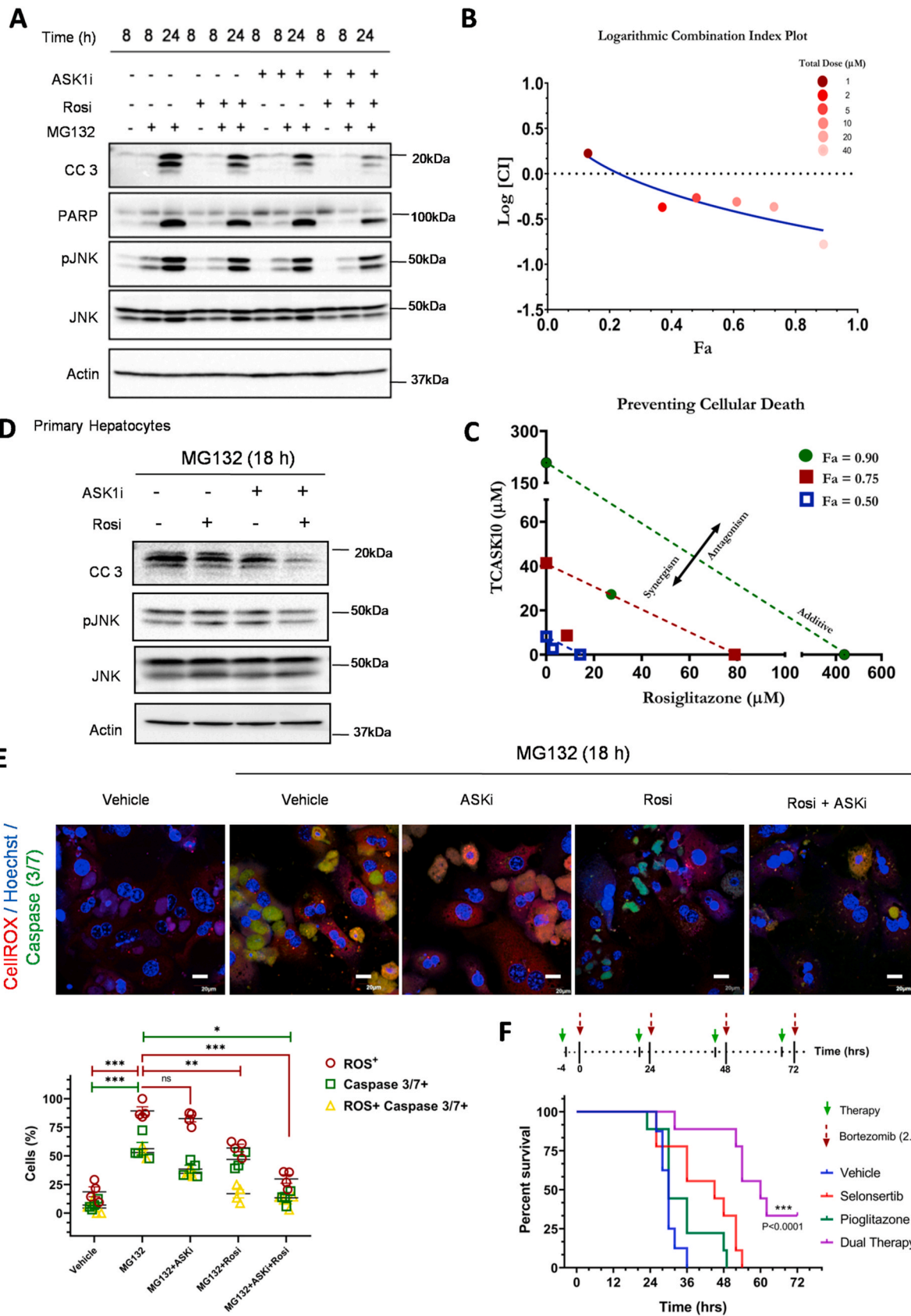
Fig. 7. ASK1 inhibition with concordant PPARγ activation synergistically protects hepatocellular death. (A) Cleaved caspase 3, PARP, and p-JNK protein expressions in HepG2 cells treated with MG132 (10 μM) in the presence and absence of Rosiglitazone (10 μM), TCASK10 (10 μM), and the combination (Rosi + TCASK10) for 8 and 24h. (B–C) HepG2 cells in triplicate pretreated with different doses of Rosiglitazone, TCASK10, and the combination (1:1; molar ratio) for 4h and with MG132 (10 μM) for the next 12 h and Live dead assay was performed. Logarithmic combination index plot (B) and Isobologram (C) for Fa 0.90 (green), 0.75 (red) and 0.50 (blue) were plotted. (D–E) Primary hepatocytes were treated with MG132 (10 μM) in the presence and absence of Rosiglitazone (10 μM), TCASK10 (10 μM), and the combination (Rosi + TCASK10) for 18h. Cleaved caspase 3, p-JNK, and JNK protein expression have been checked using immunoblot assay (D). Dual detection for ROS production (CellROX) and Apoptosis (Caspase 3/7 substrate assay) was performed using confocal microscopy. Percent of ROS$^{+(RED)}$, Caspase 3/7$^{+(GREEN)}$, and Dual$^{+(YELLOW)}$ cells were calculated (E, bottom panel) (n = 5/group, 5 fields/sample). (F) Mice (n = 9/group) were intraperitoneally administered with bortezomib (2.5 mg/kg) every 24 h for survival analysis. 4 h before each bortezomib treatment animals were given vehicle [blue], selonsertib (10 mg/kg) [red], pioglitazone (30 mg/kg) [green], and dual (selonsertib + pioglitazone) [violet] therapy. Values were presented as mean ± SEM, *P < 0.05; **P < 0.01; ***P < 0.001; ns, not significant. Scale bars, 20 μm. (For interpretation of the references to color in this figure legend, the reader is referred to the Web version of this article.)

suppresses ROS production (Supplementary Fig. 8B). Taken together, PPARγ is required for PEDF mediated antiapoptotic effects under proteotoxic stress, an effect mediated via antioxidative defense mechanism.

3.7. PPARγ sufficiency therapeutically weighs the outcome of ASK1 inhibition under hepatic proteasomal stress

We next asked whether functional PPARγ is also required for the therapeutic outcome of ASK1 inhibitors in proteasomal inhibition [49]. To this end, PPARγ in the liver was depleted by adenovirus, and mice were treated with selonsertib and bortezomib to monitor proteotoxicity (Supplementary Fig. 8C). Knockdown of PPARγ further enhanced bortezomib-induced sinusoidal dilatation, oxidative stress, hepatocellular death, and serum ALT and AST levels. Seloncertib however failed to rescue these markers of liver injury when PPARγ was knocked down (Fig. 6E–G). These results collectively suggest that PPARγ-dependent antioxidative defense system is a prerequisite for the therapeutic outcome of ASK1 inhibitors in proteotoxic stress.

3.8. Combinatorial use of ASK1 inhibitor and PPARγ activator has superior anti-apoptotic and survival response

We next tested the hypothesis that combinations of ASK1 inhibitor and PPARγ agonist would have better outcomes upon proteasomal inhibition. Co-treatment of HepG2 cells with rosiglitazone and TC ASK10 (ASK1i) exceedingly suppresses apoptosis when treated alone in a time-dependent manner (Fig. 7A). To determine the drug interactions between ASKi and Rosi for preventing MG132 induced hepatocellular death, log[CI] values were used to construct a logarithmic Combination Index plot (Fig. 7B) to elucidate whether the combinations are antagonistic (log[CI]>0), synergistic (log[CI]<0), or additive (log[CI] = 0). The drug combination at 1:1 M ratio shows synergistic interaction for all the doses except the lowest total dose (1 μM). ASKi and Rosi independently had median effective dose (ED50) of 8.21 μM and 14.25 μM, respectively, whereas the combination exhibited an ED50 of 2.74 μM as depicted by Dose-Reduction Index (DRI) data. Moreover, the Isobologram study (Fig. 7C) further demonstrated synergy between ASKi and Rosi at ED50, ED75, and ED90 (Data file S1). Consistently, when we challenged primary hepatocytes with MG132 in presence of Rosi and ASK1i, dual treatment remarkably suppressed both ROS generation and caspase3/7 activation (Fig. 7D and E). Moreover, pretreatment of selonsertib and pioglitazone combination prolonged median survival by two-fold (30 h–60 h) in the bortezomib treated mice while monotherapy did not have a significant impact on survival (Fig. 7F).

3.9. ASK1 inhibition and concomitant PPARγ activation potently block proteotoxicity and hallmarks of NASH

Both ASK1 and PPARγ have been shown to be potential targets in NASH therapy; we thereby examined the outcome of selonsertib and pioglitazone dual therapy in a mouse model of NAFLD. We gavaged selonsertib, pioglitazone, or their combination for the last four weeks of HFD feeding (Fig. 8A). The bodyweight of HFD fed and selonsertib treated mice progressively increased over sixteen weeks while

pioglitazone and combination therapy significantly slowed the rate of weight gain (Supplementary Figs. 9A and B). Fasting blood glucose levels were significantly reduced following treatments with pioglitazone or combination therapy whereas selonsertib treatment alone had no impact on fasting blood glucose (Supplementary Fig. 9B). Consistently, liver and epididymal fat pad weight were significantly low (Supplementary Figs. 9A , C, D). Insulin tolerance test (ITT) and oral glucose tolerance test (OGTT) also revealed strong insulin-sensitizing action of pioglitazone but selonsertib did not affect insulin resistance and glucose intolerance (Fig. 8B and C). In contrast, both pioglitazone and seloncertib significantly reduced serum AST and ALT levels while the combination therapy had further diminished serum markers of liver injury (Fig. 8D). Interestingly, proteasomal activity in the liver was significantly enhanced by pioglitazone and combination therapy (Fig. 8E) with a marked reduction in polyubiquitylated proteins (Fig. 8F). Combination therapy also led to a striking reduction in CC3 and PARP, two apoptosis markers (Fig. 8F). While treatment with pioglitazone significantly decreased steatosis, fibrosis, oxidative stress, and ubiquitin accumulation without an appreciable decrease in apoptosis, selonsertib in contrast remarkably diminished the number of TUNEL positive cells. Combination therapy, however, revealed significantly better resolution of NASH pathogenesis in restoring both proteastasis and hepatocellular death (Fig. 8G).

4. Discussion

Our study unraveled hepatocellular proteasomal dysfunction as one key pathological feature in diet-induced murine models and human NASH patients. While our preclinical mouse model showed a relatively homogenous decline in proteasomal activity, correlations of proteasomal genes with NASH signature genes suggest that histologically confirmed NASH is a spectrum of diseases where a subset of patients have severe proteasomal dysfunction. Moreover, acute drug-induced proteasomal inhibition and NASH share overlapping pharmacologically targetable ROS-driven molecular repertoires that induce significant liver injury.

Hepatocytes are highly sensitive to oxidative stress, an unfavorable condition where ROS generation supersedes antioxidant defense mechanisms [50]. We showed that bortezomib-induced liver injury is driven by ROS production and the activation of apoptosis. ROS-mediated cell death involves numerous pathways including p53 mediated apoptosis, mitochondrial apoptosis pathway, ER stress, autophagy, necroptosis, and anoikis often through random oxidation of cellular proteins and lipids [51]. From the transcriptomic analysis of bortezomib-treated livers, we have implicated two ROS-sensitive pathways, viz activation of pro-apoptotic ASK1-JNK-p38 pathway and downregulation of anti-oxidant Nrf2-PPARγ pathway. The redox-regulated cellular outcome is often mediated via the reversible oxidation of thiol-containing negative regulators including thioredoxin (TRX) for ASK1 and Kelch-like ECH-associated protein 1 (KEAP1) for Nrf2 [52, 53].

Although inhibition of ASK1 is critical in blocking bortezomib-mediated hepatocyte death, it, however, has no impact on cellular ROS levels. Thus simultaneous activation of antioxidant response would
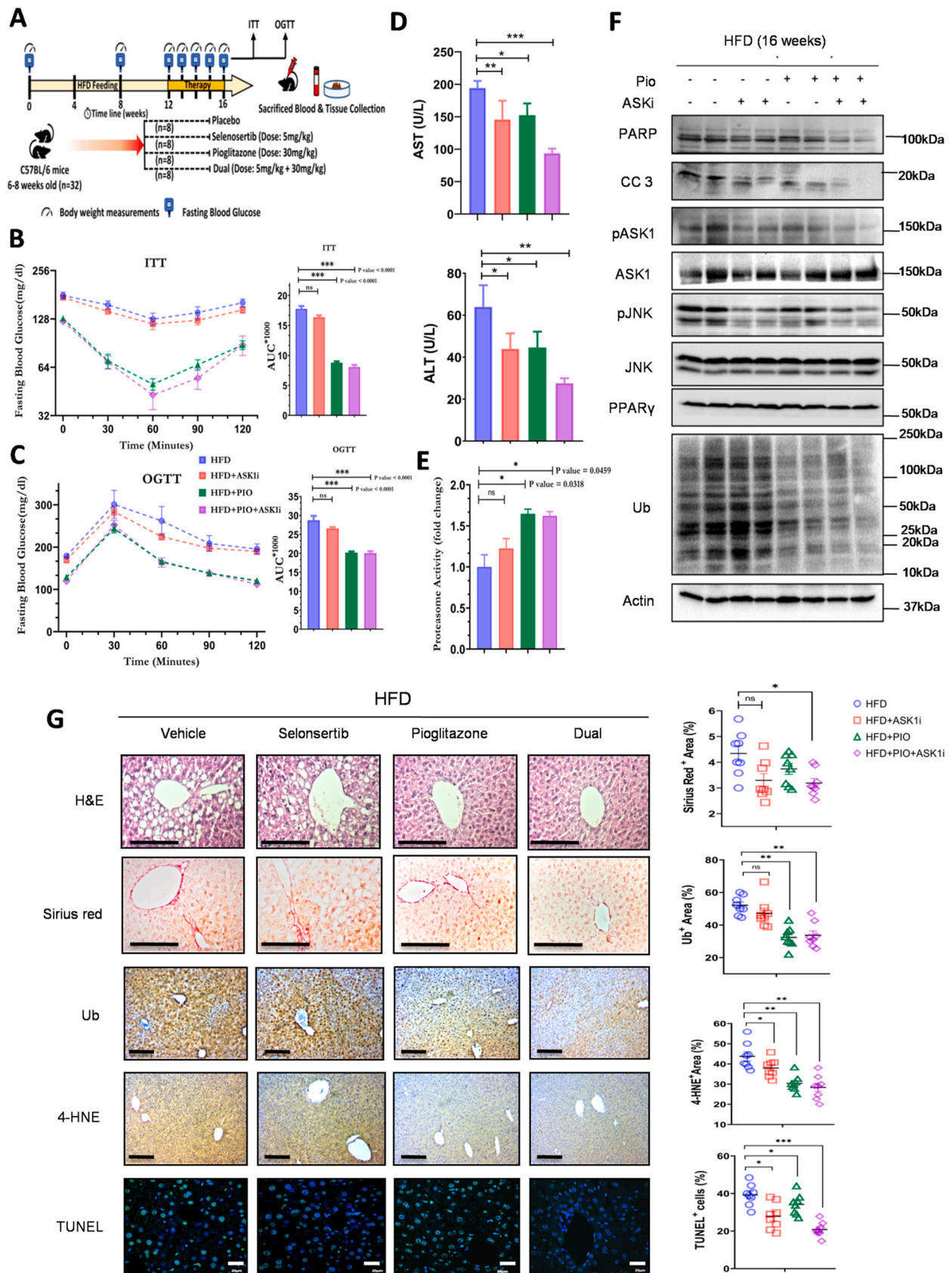
(caption on next page)

Fig. 8. Combination therapy restores proteasomal activity and improves the hallmarks of NASH. (A–C) Mice were fed with HFD for 16 weeks, randomly distributed and administered with vehicle [blue], selonsertib (10 mg/kg) [red], pioglitazone (30 mg/kg) [green], and combination (selonsertib + pioglitazone) [violet] therapy once daily for the last 4 weeks. Experimental flowchart and timeline for the experiment (A). ITT (B) and OGTT (C) were performed for the 4 treatment groups. Area Under Curve (AUC) for respective ITT and OGTT experiments were calculated (B, C; right panel). (D) Serum AST and ALT values. (E) Chymotrypsin-like proteasomal activity was measured from the liver lysates. (F) Immunoblot assays for the expression apoptosis markers (Cleaved caspase 3, PARP), ASK1 activity markers (p-ASK1, p-JNK), Ubiquitin, and PPARγ. (G) H&E, Sirius red, TUNEL assay and immunohistochemistry for 4-HNE, Ubiquitin performed. Sirius red, 4-HNE, Ubiquitin positive area (%), and percent TUNEL$^+$ cells were quantified (Right panels; n = 8/group, 5 fields/sample). Values were presented as mean ± SEM, *P < 0.05; **P < 0.01; ***P < 0.001; ns, not significant. Scale bars, 100 μm (Histology); 20 μm (TUNEL). (For interpretation of the references to color in this figure legend, the reader is referred to the Web version of this article.)

further accentuate response to ASK1 inhibition. Our results indicate that PPARγ provides the basal antioxidative defense machinery where ASK1i can efficiently work. Moreover, PEDF an endogenous activator of PPARγ also showed hepatoprotective effects under proteasomal inhibition suggesting a functional hepatic PEDF-PPARγ pathway as an attractive therapeutic target. Besides, ASKi did not restore proteasomal activity and inhibit the accumulation of ubiquitylated proteins in HFD fed mice suggesting ASK1 functions downstream of proteasome inhibition and ROS production. Thus, a combination of ASK1i and PPARγ agonist conspicuously impedes bortezomib-induced liver injury and prolongs survival. This drug combination turns out to be clinically attractive as they show pharmacological synergism.

Failure of several monotherapy trials calls for developing effective combination therapy in NASH underscoring its complex multifaceted pathophysiology of insulin resistance, cellular death, inflammation, and fibrosis. Insulin-sensitizing PPARγ agonism showed several untoward side effects such as adipogenesis and weight gain, while PPARγ agonists have been reported to improve liver injury and fibrosis in NASH patients [54,55]. Our study not only emphasizes the prime importance of hepatic PPARγ in restoring the innate redox homeostasis under proteasome-associated metabolic stress but also proposes that the combination therapy of selonsertib and pioglitazone holds promising translational potential in mitigating NASH by tuning the balance between two overlapping molecular repertoires associated with liver injury and redox driven metabolic homeostasis.

Bortezomib has been frequently used for treating multiple myeloma patients as standard chemotherapeutic regimen. Besides the most frequent general side effects such as gastrointestinal discomfort, neuropathy, and thrombocytopenia, several cases of fatal liver failure, cholestasis, and recurrent acute hepatitis have also been reported in recent times [10,11,56]. Our preclinical data thereby suggests the use of this combination therapy as a novel therapeutic opportunity for treating bortezomib-induced acute hepatotoxicity in multiple myeloma patients.

5. Conclusions

Collectively, our results show that both human and murine NASH and acute drug-induced proteasomal inhibition share overlapping pharmacologically targetable molecular repertoires that induce significant liver injury. Precisely, activation of ASK1 with a concomitant insufficient PPARγ driven antioxidant response underlies proteotoxic liver injury and a combination therapy targeting ASK1 and PPARγ confers robust protection against drug-induced liver injury and ameliorates NASH in a preclinical model.

Declaration of competing interest

The authors have declared that no conflict of interest exists.

Acknowledgments

Appendix A. Supplementary data

Supplementary data to this article can be found online at https://doi.org/10.1016/j.redox.2021.102043.

Author contributions

DD and AP performed most of the cell-based and animal experiments. DD and MA conducted proteasomal inhibition experiments. DD and SKM conducted primary hepatocyte experiments. DD and AS have generated purified recombinant adenoviruses and adeno-associated viruses. AL and SP conducted all the transcriptomic data analysis. DD, SP, and PC analyzed the data and wrote the paper.

Data and materials availability

Mouse transcriptomic data are available at the GEO repository (Accession number: GSE164508).

References

[1] U. Tomaru, S. Takahashi, A. Ishizu, Y. Miyatake, A. Gohda, S. Suzuki, A. Ono, J. Ohara, T. Baba, S. Murata, K. Tanaka, M. Kasahara, Decreased proteasomal activity causes age-related phenotypes and promotes the development of metabolic abnormalities, Am. J. Pathol. 180 (2012) 963–972.

[2] T.M. Donohue, N.A. Osna, K.K. Kharbanda, P.G. Thomes, Lysosome and proteasome dysfunction in alcohol-induced liver injury, Liver Res 3 (2019) 191–205.

[3] M. Takagi, M. Yamauchi, G. Toda, K. Takada, T. Hirakawa, K. Ohkawa, Serum ubiquitin levels in patients with alcoholic liver disease, in: Alcohol. Clin. Exp. Res. vol. 23, Lippincott Williams and Wilkins, 1999, pp. 76S–80S, 4 Suppl.

[4] C. Lebeaupin, D. Vallée, Y. Hazari, C. Hetz, E. Chevet, B. Bailly-Maitre, al, Endoplasmic, endoplasmic reticulum stress signaling and the pathogenesis of non-alcoholic fatty liver disease, J. Hepatol. 69 (2018).

[5] K. Gariani, K.J. Menzies, D. Ryu, C.J. Wegner, X. Wang, E.R. Ropelle, N. Moullan, H. Zhang, A. Perino, V. Lemos, B. Kim, Y.K. Park, A. Piersigilli, T.X. Pham, Y. Yang, C.S. Ku, S.I. Koo, A. Fomitchova, C. Cantó, K. Schoonjans, A.A. Sauve, J.Y. Lee, J. Auwerx, Eliciting the mitochondrial unfolded protein response by nicotinamide adenine dinucleotide repletion reverses fatty liver disease in mice, Hepatology 63 (2016) 1190–1204.

[6] S. Tanaka, H. Hikita, T. Tatsumi, R. Sakamori, Y. Nozaki, S. Sakane, Y. Shiode, T. Nakabori, Y. Saito, N. Hiramatsu, K. Tabata, T. Kawabata, M. Hamasaki, H. Eguchi, H. Nagano, T. Yoshimori, T. Takehara, Rubicon inhibits autophagy and accelerates hepatocyte apoptosis and lipid accumulation in nonalcoholic fatty liver disease in mice, Hepatology 64 (2016) 1994–2014.

[7] T. Otoda, T. Takamura, H. Misu, T. Ota, S. Murata, H. Hayashi, H. Takayama, A. Kikuchi, T. Kanamori, K.R. Shima, F. Lan, T. Takeda, S. Kurita, K. Ishikura, Y. Kita, K. Iwayama, K.I. Kato, M. Uno, Y. Takeshita, M. Yamamoto, K. Tokuyama, S. Iseki, K. Tanaka, S. Kaneko, Proteasome dysfunction mediates obesity-induced endoplasmic reticulum stress and insulin resistance in the liver, Diabetes 62 (2013) 811–824.

[8] Y. Kim, K.Y. Kim, S.H. Lee, Y.Y. Chung, S.-A. Yahng, S.-E. Lee, G. Park, C.-K. Min, A case of drug-induced hepatitis due to bortezomib in multiple myeloma, Immune Netw 12 (2012) 126.

[9] A. Garg, M. Morgunskyy, Y. Belagali, N. Gupta, S.P. Akku, Management of multiple myeloma and usage of bortezomib: perspective from India and Ukraine, Front. Oncol. 6 (2016) 243.

[10] L. Rosiñol, S. Montoto, M.T. Cibeira, J. Bladé, Bortezomib-induced severe hepatitis in multiple myeloma: a case report, Arch. Intern. Med. 165 (2005) 464–465.

[11] T. Cornelis, E.A.M. Beckers, A.L.C. Driessen, F.M. Van Der Sande, G.H. Koek, Bortezomib-associated fatal liver failure in a haemodialysis patient with multiple myeloma, Clin. Toxicol. 50 (2012) 444–445.

[12] R. Koschny, T.M. Ganten, J. Sykora, T.L. Haas, M.R. Sprick, A. Kolb, W. Stremmel, H. Walczak, TRAIL/Bortezomib cotreatment is potentially hepatotoxic but induces cancer-specific apoptosis within a therapeutic window, Hepatology 45 (3) (2007 Mar) 649–658.

[13] J. Hanna, A. Meides, D.P. Zhang, D. Finley, A ubiquitin stress response induces altered proteasome composition, Cell 129 (2007) 747–759.

[14] B.F. Banner, L. Savas, J. Zivny, K. Tortorelli, H.L. Bonkovsky, Ubiquitin as a marker of cell injury in nonalcoholic steatohepatitis, Am. J. Clin. Pathol. 114 (2000) 860–866.

[15] V. Cohen-Kaplan, I. Livneh, N. Avni, B. Fabre, T. Ziv, Y.T. Kwon, A. Ciechanover, p62- and ubiquitin-dependent stress-induced autophagy of the mammalian 26S proteasome, Proc. Natl. Acad. Sci. U. S. A 113 (2016) E7490–E7499.

[16] K. Zhu, K. Dunner, D.J. McConkey, Proteasome inhibitors activate autophagy as a cytoprotective response in human prostate cancer cells, Oncogene 29 (2010) 451–462.

[17] C. Espinosa-Diez, V. Miguel, D. Mennerich, T. Kietzmann, P. Sánchez-Pérez, S. Cadenas, S. Lamas, Antioxidant responses and cellular adjustments to oxidative stress, Redox Biol 6 (2015) 183–197.

[18] E.B. Kurutas, The importance of antioxidants which play the role in cellular response against oxidative/nitrosative stress: current state, Nutr. J. 15 (2016).

[19] I. Milisav, B. Poljšak, S. Ribarič, Reduced risk of apoptosis: mechanisms of stress responses, Apoptosis 22 (2017) 265–283.

[20] S. Emanuele, G. Calvaruso, M. Lauricella, M. Giuliano, G. Bellavia, A. D`Anneo, R. Vento, G. Tesoriere, Apoptosis induced in hepatoblastoma HepG2 cells by the proteasome inhibitor MG132 is associated with hydrogen peroxide production, expression of Bcl-XS and activation of caspase-3, Int. J. Oncol. 21 (2002) 857–865.

[21] A. Anan, E.S. Baskin-Bey, S.F. Bronk, N.W. Werneburg, V.H. Shah, G.J. Gores, Proteasome inhibition induces hepatic stellate cell apoptosis, Hepatology 43 (2) (2006 Feb) 335–344.

[22] B. Pandit, A.L. Gartel, Tumorigenesis and neoplastic progression proteasome inhibitors induce p53-independent apoptosis in human cancer cells, Am. J. Pathol. 178 (2011) 355–360.

[23] J.-A. Pan, E. Ullman, Z. Dou, W.-X. Zong, Inhibition of protein degradation induces apoptosis through a microtubule-associated protein 1 light chain 3-mediated activation of caspase-8 at intracellular membranes, Mol. Cell Biol. 31 (2011) 3158–3170.

[24] C.M. Westerberg, H. Hägglund, G. Nilsson, Proteasome inhibition upregulates Bim and induces caspase-3-dependent apoptosis in human mast cells expressing the Kit D816V mutation, Cell Death Dis. 3 (2012) 417.

[25] T. Mao, M. Shao, Y. Qiu, J. Huang, Y. Zhang, B. Song, Q. Wang, L. Jiang, Y. Liu, J. D.J. Han, P. Cao, J. Li, X. Gao, L. Rui, L. Qi, W. Li, Y. Liu, PKA phosphorylation couples hepatic inositol-requiring enzyme 1α to glucagon signaling in glucose metabolism, Proc. Natl. Acad. Sci. U. S. A 108 (2011) 15852–15857.

[26] T.C. Chou, P. Talalay, Quantitative analysis of dose-effect relationships: the combined effects of multiple drugs or enzyme inhibitors, Adv. Enzym. Regul. 22 (1984) 27–55.

[27] T.C. Chou, Theoretical basis, experimental design, and computerized simulation of synergism and antagonism in drug combination studies, Pharmacol. Rev. 58 (2006) 621–681.

[28] A.D. Yates, P. Achuthan, W. Akanni, J. Allen, J. Allen, J. Alvarez-Jarreta, M. R. Amode, I.M. Armean, A.G. Azov, R. Bennett, J. Bhai, K. Billis, S. Boddu, J. C. Marugán, C. Cummins, C. Davidson, K. Dodiya, R. Fatima, A. Gall, C.G. Giron, L. Gil, T. Grego, L. Haggerty, E. Haskell, T. Hourlier, O.G. Izuogu, S.H. Janacek, T. Juettemann, M. Kay, I. Lavidas, T. Le, D. Lemos, J.G. Martinez, T. Maurel, M. McDowall, A. McMahon, S. Mohanan, B. Moore, M. Nuhn, D.N. Oheh, A. Parker, A. Parton, M. Patricio, M.P. Sakthivel, A.I. Abdul Salam, B.M. Schmitt, H. Schuilenburg, D. Sheppard, M. Sycheva, M. Szuba, K. Taylor, A. Thormann, G. Threadgold, A. Vullo, B. Walts, A. Winterbottom, A. Zadissa, M. Chakiachvili, B. Flint, A. Frankish, S.E. Hunt, G. Iisley, M. Kostadima, N. Langridge, J. E. Loveland, F.J. Martin, J. Morales, J.M. Mudge, M. Muffato, E. Perry, M. Ruffier, S.J. Trevanion, F. Cunningham, K.L. Howe, D.R. Zerbino, P. Flicek, Ensembl 2020, Nucleic Acids Res 48 (2020) D682–D688.

[29] M. Lawrence, W. Huber, H. Pagès, P. Aboyoun, M. Carlson, R. Gentleman, M. T. Morgan, V.J. Carey, Software for computing and annotating genomic ranges, PLoS Comput. Biol. 9 (2013).

[30] M.I. Love, W. Huber, S. Anders, Moderated estimation of fold change and dispersion for RNA-seq data with DESeq2, Genome Biol. 15 (2014) 550.

[31] G. Korotkevich, V. Sukhov, A. Sergushichev, Fast Gene Set Enrichment Analysis, BioRxiv., 2016, 060012.

[32] D.J. McCarthy, Y. Chen, G.K. Smyth, Differential expression analysis of multifactor RNA-Seq experiments with respect to biological variation, Nucleic Acids Res. 40 (2012) 4288–4297.

[33] M.P. Suppli, K.T.G. Rigbolt, S.S. Veidal, S. Heebøll, X. Peter, L. Eriksen, M. Demant, J.I. Bagger, J.C. Nielsen, D. Oró, S.W. Thrane, A. Lund, C. Strandberg, M.J. Kønig, T. Vilsbøll, N. Vrang, K.L. Thomsen, H. Grønbaek, J. Jelsing, H.H. Hansen, F. K. Knop, Hepatic transcriptome signatures in patients with varying degrees of nonalcoholic fatty liver disease compared with healthy normal-weight individuals, Am. J. Physiol. Gastrointest. Liver Physiol. 316 (2019) 462–472.

[34] A. Liberzon, A. Subramanian, R. Pinchback, H. Thorvaldsdottir, P. Tamayo, J. P. Mesirov, Molecular signatures database (MSigDB) 3.0, Bioinformatics 27 (2011) 1739–1740.

[35] G. Fujino, T. Noguchi, K. Takeda, H. Ichijo, Thioredoxin and protein kinases in redox signaling, Semin. Canc. Biol. 16 (2006) 427–435.

[36] A. Matsuzawa, K. Saegusa, T. Noguchi, C. Sadamitsu, H. Nishitoh, S. Nagai, S. Koyasu, K. Matsumoto, K. Takeda, H. Ichijo, ROS-dependent activation of the TRAF6-ASK1-p38 pathway is selectively required for TLR4-mediated innate immunity, Nat. Immunol. 6 (2005) 587–592.

[37] S. Schuster-Gaul, L.J. Geisler, M.D. McGeough, C.D. Johnson, A. Zagorska, L. Li, A. Wree, V. Barry, I. Mikaelian, L.J. Jih, B.G. Papouchado, G. Budas, H. M. Hoffman, A.E. Feldstein, ASK1 inhibition reduces cell death and hepatic fibrosis in an Nlrp3 mutant liver injury model, JCI Insight 5 (2020).

[38] R. Loomba, E. Lawitz, P.S. Mantry, S. Jayakumar, S.H. Caldwell, H. Arnold, A. M. Diehl, C.S. Djedjos, L. Han, R.P. Myers, G.M. Subramanian, J.G. McHutchison, Z.D. Goodman, N.H. Afdhal, M.R. Charlton, The ASK1 inhibitor selonsertib in patients with nonalcoholic steatohepatitis: a randomized, phase 2 trial, Hepatology 67 (2018) 549–559.

[39] S.A. Harrison, V.W.S. Wong, T. Okanoue, N. Bzowej, R. Vuppalanchi, Z. Younes, A. Kohli, S. Sarin, S.H. Caldwell, N. Alkhouri, M.L. Shiffman, M. Camargo, G. Li, K. Kersey, C. Jia, Y. Zhu, C.S. Djedjos, G.M. Subramanian, R.P. Myers, N. Gunn, A. Sheikh, Q.M. Anstee, M. Romero-Gomez, M. Trauner, Z. Goodman, E.J. Lawitz, Z. Younossi, Selonsertib for patients with bridging fibrosis or compensated cirrhosis due to NASH: results from randomized phase III STELLAR trials, J. Hepatol. 73 (2020) 26–39.

[40] X. Wang, X. Liu, Y. Ren, Y. Liu, S. Han, J. Zhao, X. Gou, Y. He, PEDF protects human retinal pigment epithelial cells against oxidative stress via upregulation of UCP2 expression, Mol. Med. Rep. 19 (2019) 59–74.

[41] M. Adak, D. Das, S. Niyogi, C. Nagalakshmi, D. Ray, P. Chakrabarti, Inflammasome activation in Kupffer cells confers a protective response in nonalcoholic steatohepatitis through pigment epithelium-derived factor expression, [published online ahead of print, 2018 Jun 13], Faseb. J. (2018), fj201800190.

[42] Y. Ishibashi, T. Matsui, K. Ohta, R. Tanoue, M. Takeuchi, K. Asanuma, K. Fukami, S. Okuda, K. ichiro Nakamura, S. ichi Yamagishi, PEDF inhibits AGE-induced podocyte apoptosis via PPAR-gamma activation, Microvasc. Res. 85 (2013) 54–58.

[43] C. Zhu, X. Zhang, H. Qiao, L. Wang, X. Zhang, Y. Xing, C. Wang, L. Dong, Y. Ji, X. Cao, The intrinsic PEDF is regulated by PPARγ in permanent focal cerebral ischemia of rat, Neurochem. Res. 37 (2012) 2099–2107.

[44] C. Lee, Collaborative power of Nrf2 and PPAR γ activators against metabolic and drug-induced oxidative injury, Oxid. Med. Cell. Longev. 2017 (2017) 1378175.

[45] S. Polvani, M. Tarocchi, A. Galli, PPAR and oxidative stress: con(β) catenating NRF2 and FOXO, PPAR Res. 2012 (2012) 641087.

[46] L. Hecker, N.J. Logsdon, D. Kurundkar, A. Kurundkar, K. Bernard, T. Hock, E. Meldrum, Y.Y. Sanders, V.J. Thannickal, Reversal of persistent fibrosis in aging by targeting Nox4-Nrf2 redox imbalance, Sci. Transl. Med. 6 (2014) 231ra47, 231ra47.

[47] Y. Lu, Y. Sun, Z. Liu, Y. Lu, X. Zhu, B. Lan, Z. Mi, L. Dang, N. Li, W. Zhan, L. Tan, J. Pi, H. Xiong, L. Zhang, Y. Chen, Activation of NRF2 ameliorates oxidative stress and cystogenesis in autosomal dominant polycystic kidney disease, Sci. Transl. Med. 12 (2020) 3613.

[48] X. Chen, H. Xue, W. Fang, K. Chen, S. Chen, W. Yang, T. Shen, X. Chen, P. Zhang, W. Ling, Adropin protects against liver injury in nonalcoholic steatohepatitis via the Nrf2 mediated antioxidant capacity, Redox Biol 21 (2019).

[49] C. Ugbode, N. Garnham, L. Fort-Aznar, G.J.O. Evans, S. Chawla, S.T. Sweeney, JNK signalling regulates antioxidant responses in neurons, Redox Biol 37 (2020) 101712.

[50] V. Azzimato, J. Jager, P. Chen, C. Morgantini, L. Levi, E. Barreby, A. Sulen, C. Oses, J. Willerbrords, C. Xu, X. Li, J.X. Shen, N. Akbar, L. Haag, E. Ellis, K. Wålhen, E. Näslund, A. Thorell, R.P. Choudhury, V.M. Lauschke, M. Rydén, S.M. Craige, M. Aouadi, Liver macrophages inhibit the endogenous antioxidant response in obesity-associated insulin resistance, Sci. Transl. Med. 12 (2020).

[51] M. Redza-Dutordoir, D.A. Averill-Bates, Activation of apoptosis signalling pathways by reactive oxygen species, Biochim. Biophys. Acta Mol. Cell Res. 1863 (2016) 2977–2992.

[52] M. Soga, A. Matsuzawa, H. Ichijo, Oxidative stress-induced diseases via the ASK1 signaling pathway, Int. J. Cell Biol. 2012 (2012) 439587.

[53] I. Bellezza, I. Giambanco, A. Minelli, R. Donato, Nrf2-Keap1 signaling in oxidative and reductive stress, Biochim. Biophys. Acta Mol. Cell Res. 1865 (2018) 721–733.

[54] G.P. Aithal, J.A. Thomas, P.V. Kaye, A. Lawson, S.D. Ryder, I. Spendlove, A. S. Austin, J.G. Freeman, L. Morgan, J. Webber, Randomized, placebo-controlled trial of pioglitazone in nondiabetic subjects with nonalcoholic steatohepatitis, Gastroenterology 135 (2008) 1176–1184.

[55] J. Skat-Rørdam, D. Højland Ipsen, J. Lykkesfeldt, P. Tveden-Nyborg, A role of peroxisome proliferator-activated receptor γ in non-alcoholic fatty liver disease, Basic Clin. Pharmacol. Toxicol. 124 (2019) 528–537.

[56] A. Jain, P. Malhotra, V. Suri, S. Varma, A. Das, S. Mitra, Cholestasis in a patient of multiple myeloma: a rare occurrence of bortezomib induced liver injury, Indian J. Hematol. Blood Transfus. 32 (2016) 181–183.